

# The lensing efficiencies of MACS X-ray selected versus RCS optically selected galaxy clusters

A. Horesh,<sup>1\*</sup> D. Maoz,<sup>1</sup> H. Ebeling,<sup>2</sup> G. Seidel,<sup>3</sup> and M. Bartelmann<sup>3</sup>

<sup>1</sup>*School of Physics and Astronomy, Tel Aviv University, Tel Aviv 69978, Israel*

<sup>2</sup>*Institute for Astronomy, University of Hawaii, 2680 Woodlawn Drive, Honolulu, HI 96822, USA*

<sup>3</sup>*Zentrum für Astronomie der Universität Heidelberg, Institut für Theoretische Astrophysik, Albert-Überle-Str. 2, 69120 Heidelberg, Germany*

13 November 2021

## ABSTRACT

The statistics of strongly lensed arcs in samples of galaxy clusters provide information on cluster structure that is complementary to that from individual clusters. However, samples of clusters that have been analyzed to date have been either small, heterogeneous, or observed with limited angular resolution. We measure the lensed-arc statistics of 97 clusters imaged at high angular resolution with the Hubble Space Telescope, identifying lensed arcs using two automated arc detection algorithms. The sample includes similar numbers of X-ray selected (MACS) and optically selected (RCS) clusters, and spans cluster redshifts in the range  $0.2 < z < 1$ . We compile a catalogue of 42 arcs in the X-ray selected subsample and 7 arcs in the optical subsample. All but five of these arcs are reported here for the first time. At  $0.3 \leq z \leq 0.7$ , the X-ray selected clusters have a significantly higher mean frequency of arcs,  $1.2 \pm 0.2$  per cluster, versus  $0.2 \pm 0.1$  in the optical sample. The strikingly different lensing efficiencies indicate that X-ray clusters trace much larger mass concentrations, despite the similar optical luminosities of the X-ray and optical clusters. The mass difference is supported also by the lower space density of the X-ray clusters, and by the small Einstein radii of the few arcs in the optical sample. Higher-order effects, such as differences in concentration or substructure, may also contribute.

**Key words:** gravitational lensing – galaxies: clusters: general

## 1 INTRODUCTION

Galaxy clusters are natural laboratories for studying a variety of astrophysical processes and for testing cosmological models. In particular, the masses and mass profiles of clusters have proved to be useful for constraining cosmological parameters (e.g. Bridle et al. 1999; Reiprich & Böhringer 2002; Voit 2005; Allen et al. 2008; Vikhlinin et al. 2009). Gravitational lensing is frequently used to map the evolution of cluster mass profiles, ellipticities, and substructure. One approach is to perform detailed modeling of individual clusters using strong and weak lensing (e.g., Abdelsalam et al. 1998; Broadhurst et al. 2005; Leonard et al. 2007; Limousin et al. 2007; Richard et al. 2007). However, since this kind of approach requires deep data for individual clusters that exhibit numerous lensed images, the results may not be representative of the vast majority of clusters. A complementary approach is to measure the statistics of lensed arcs in large samples of clusters. Lensing statistics thus provide another means to study clusters as a population.

For the past decade there has been debate concerning theoretical lensing statistics predictions and their confrontation with observations. Bartelmann et al. (1998; B98) performed lensing simulations using artificial sources at redshift  $z = 1$  by ray tracing through the five most massive clusters formed in a cosmological N-body dark matter simulation (Kauffmann et al. 1999). The observed number of giant arcs, with length-to-width ratio  $l/w \geq 10$  and  $R < 21.5$  mag, present over the whole sky was estimated by extrapolating from observations of a subsample of X-ray selected clusters from the Einstein Extended Medium Sensitivity Survey (EMSS), and compared to the theoretical calculation. B98 found that the estimated number of observed arcs is larger by almost an order of magnitude than the number predicted by the now-standard  $\Lambda$ CDM model. Later estimates of lensed arcs statistics in clusters from both the Las Campanas Distant Cluster Survey (Zaritsky & Gonzales 2003; arcs with  $l/w \geq 10$  and  $R < 21.5$  mag) and the Red-Sequence Cluster Survey (RCS; Gladders et al. 2003) confirmed the estimates of the observed number of arcs derived by B98. Most recently, Hennawi et al. (2008) analyzed a sample of 240 clusters, optically selected from the Sloan Digital Sky Survey (SDSS), and found that 10% – 20% of them are strong lenses, similar to the find-

\* E-mail: assafh@wise.tau.ac.il

ings of Gladders et al. (2003). The largest catalogue of arcs to date was compiled by Sand et al. (2005) who found 104 arcs in 128 clusters. However, their systematic search for arcs was performed on a largely heterogeneous cluster sample.

The apparent overproduction of arcs by real clusters has stimulated further theoretical studies of arc statistics. Meneghetti et al. (2000) studied numerically the effect of the masses of the individual cluster galaxies on a cluster's lensing cross section, and found it to be negligible, as also found in a study by Flores, Maller, & Primack (2000). However, the increase in lensing cross section due to the central cluster cD galaxy may be as high as  $\sim 50\%$  (Meneghetti, Bartelmann, & Moscardini 2003) and the increase in cross section due to the intra-cluster gas could perhaps be by a factor of a few (Puchwein et al. 2005, Rozo et al. 2008). Oguri, Lee, & Suto (2003) argued that halo triaxiality could also play an important role in increasing cluster lensing cross sections. Torri et al. (2004) raised the possibility that X-ray selection of clusters may favor merging systems, which may be more efficient lenses. Wambsganss, Bode, & Ostriker (2004) pointed out that since lensing cross section is a steep function of source redshift, the conflict between theory and observations could be the result of the assumed source redshifts in the simulations. Similarly, Dalal, Holder, & Hennawi (2004) performed a lensing simulation using artificial background sources at different redshifts and a large sample of simulated clusters. They found that their prediction for the number of lensed arcs was consistent with an observed number that they derived from a sample of X-ray selected EMSS clusters. The difference between this result and that of B98 was explained by the combination of three main effects: the inclusion of sources at different redshifts; the use of a higher source density in the Dalal et al. simulation; and an observed cluster number density lower than the one used by B98 for estimating the all-sky number of arcs.

A more observationally oriented approach to lensing statistics simulations was introduced by Horesh et al. (2005; H05) in order to test specifically the lensing efficiency of individual clusters, independent of the separate question of the number density of clusters. H05 repeated the B98 simulations using the same simulated clusters, but using background sources from the Hubble Deep Field (HDF), each at a redshift based on its actual photometric redshift. Observational effects including background, photon noise, and the light of cluster galaxies were added to the simulated lensed images. A mass-matched sample of 10 X-ray-selected clusters (Smith et al. 2005) observed at high angular resolution with the Hubble Space Telescope (HST) was used for comparison with the simulated sample. Finally, an automated objective arc-detection algorithm was applied to both the observed and the simulated samples. This procedure permitted measuring and comparing the frequency of arcs over a larger range in magnitudes (down to  $R \leq 24$  mag). H05 found that the lensing efficiency of their simulated clusters at  $z \approx 0.2$  was consistent, to within Poisson errors, with that of their observed sample. While the analysis suggested that the observed clusters could be somewhat more efficient lenses by up to a factor of two, this conclusion was limited by the small size of both the observed and the simulated samples, as well as the parameters assumed in the simulations.

Indeed, an important parameter that affects all theoretical studies of arc statistics is  $\sigma_8$ , the overdensity within an 8 Mpc radius comoving sphere. Past simulations have used diverse values: 0.9 (B98; Dalal et al. 2004; H05) or 0.95 (Wambsganss et al. 2004; Hennawi et al. 2007). Fedeli et al. (2008) have recently analyzed the effect of  $\sigma_8$  on the arc statistics question, and pointed out that the most recent values of  $\sigma_8$  from WMAP5 ( $0.796 \pm 0.036$ ; Dunk-

ley et al. 2009) revive and reinforce the discrepancy between theory and observations of arc statistics.

A possibly related debate has emerged recently on the subject of the size of the Einstein radius in clusters. Broadhurst and Barkana (2008) calculated the distribution of Einstein radii in clusters with a spherical Navarro, Frenk, & White (NFW; 1996) profile, and with a concentration distribution according to Neto et al. (2007). They compared their prediction with the observed Einstein radii of three clusters, among them Abell 1689, and found that the observed radii are significantly larger than the theoretical expectation. Yet another cluster with a large Einstein radius was recently reported by Zitrin et al. (2009). Sadeh & Rephaeli (2008) have calculated the concentration distribution of clusters based on the distribution of cluster formation times. They too find a discrepancy, albeit weak, between the observed Einstein radius of Abell 1689 and its expected value. Oguri & Blandford (2009), however, argue that the Einstein radius they obtain using a generalized triaxial form of the NFW profile (Jing & Suto 2002) is consistent with that observed in Abell 1689. In addition, they provide a prediction for the distribution of Einstein radii, which can be tested with a large statistical cluster sample.

Clearly, resolution of these problems requires, on the theoretical side, improved simulations, incorporating the most realistic cosmological parameters, source parameters, and observational effects; and from the observational perspective, large, well-understood samples of clusters at various redshifts, selected by diverse methods and uniformly observed at the high depth and resolution needed for the clear detection of large arcs.

In this paper, we address this observational perspective. We explore the observed statistical properties of 97 galaxy clusters imaged with HST. This cluster sample is large enough to be separated into several subsamples based on redshift and selection type. We apply two different arc detection algorithms to the clusters, and compile a high-resolution arc catalogue. We then study the arc statistics in the various subsamples. In a forthcoming publication, we will compare the observed statistics of this sample to new, improved, calculations of matched simulated samples. Throughout this paper we adopt a  $\Lambda$ CDM cosmology with parameters  $\Omega_m = 0.3$ ,  $\Omega_\Lambda = 0.7$ , and  $H_0 = 70 \text{ km s}^{-1} \text{ Mpc}^{-1}$ . Magnitudes are in the Vega system.

## 2 CLUSTER SAMPLES AND ANALYSIS

We have compiled from the HST archive a sample of clusters observed with the Advanced Camera for Surveys (ACS). The ACS has a field of view  $3'3 \times 3'3$ , a pixel scale of  $0''.05$ , and a point-spread function full width at half maximum of  $\approx 0''.1$ .

Among the clusters in our sample, 35 are from the MASSive Cluster Survey (MACS; Ebeling, Edge, & Henry, 2001), and 52 are from the Red-Sequence Cluster Survey (RCS; Gladders & Yee, 2005). To these we add the 10 clusters of Smith et al. (2005), observed with WFPC2, and already analyzed in H05, for a total of 97 clusters. Each of the three WFPC2 WF CCDs had a FOV of  $1'3 \times 1'3$  and a pixel scale of  $0''.1$ . We begin with a brief summary of the relevant details of each of these surveys.

### 2.1 The MASSive Cluster Survey (MACS)

MACS (Ebeling et al., 2001) has provided a statistically complete, X-ray selected sample of the most X-ray luminous galaxy clusters at  $z > 0.3$ . Based on sources detected in the Röntgen Satel-

**Table 1.** MACS low-redshift ( $0.3 \leq z < 0.5$ ) sample

Cluster	RA	Dec	$z$ (ref)	BCG $m_{F606W}$
MACSJ0035.4–2015	00:35:26.2	−20 : 15 : 44.2	... (1)	19.55
MACSJ0916.1–0023	09:16:11.5	−00 : 23 : 46.6	... (1)	—
MACSJ0140.0–0555	01:40:00.9	−05 : 55 : 02.0	... (1)	20.25
MACSJ0140.0–3410	01:40:05.6	−34 : 10 : 39.7	... (1)	19.91
MACSJ0152.5–2852	01:52:34.4	−28 : 53 : 37.4	... (1)	20.32
MACSJ0451.9+0006	04:51:54.7	+00 : 06 : 17.3	0.430 (2)	20.16
MACSJ0520.7–1328	05:20:42.0	−13 : 28 : 47.6	... (1)	19.29
MACSJ0712.3+5931	07:12:20.4	+59 : 32 : 20.8	0.328 (2)	19.00
MACSJ0845.4+0327	08:45:27.8	+03 : 27 : 38.8	... (1)	19.26
MACSJ0947.2+7623	09:47:13.2	+76 : 23 : 12.7	0.345 (3)	18.89
MACSJ0949.8+1708	09:49:51.8	+17 : 07 : 08.8	... (1)	19.81
MACSJ1006.9+3200	10:06:54.7	+32 : 01 : 32.3	... (1)	19.36
MACSJ1115.2+5320	11:15:14.8	+53 : 19 : 54.6	... (1)	19.68
MACSJ1115.8+0129	11:15:51.9	+01 : 29 : 54.2	0.355 (3)	19.52
MACSJ1133.2+5008	11:33:13.3	+50 : 08 : 39.1	0.389 (4)	19.64
MACSJ1206.2–0847	12:06:12.2	−08 : 48 : 04.4	0.440 (5)	19.92
MACSJ1236.9+6311	12:36:58.8	+63 : 11 : 12.2	0.302 (4)	18.91
MACSJ1258.0+4702	12:58:02.1	+47 : 02 : 53.5	... (1)	19.64
MACSJ1319.9+7003	13:20:08.5	+70 : 04 : 39.0	... (1)	19.07
MACSJ1354.6+7715	13:54:30.6	+77 : 15 : 20.9	0.396 (4)	—
MACSJ1652.3+5534	16:52:18.8	+55 : 34 : 56.5	... (1)	19.27
MACSJ2135.2–0102	21:35:12.1	−01 : 02 : 57.2	0.33 (6)	19.24
MACSJ2243.3–0935	22:43:20.2	−09 : 35 : 26.9	... (1)	—

Notes - Last column gives the magnitude of the brightest cluster galaxy. Redshift references: (1) Ebeling et al., in preparation; (2) Stott et al. (2007); (3) Allen et al. (2008); (4) Edge et al. (2003); (5) Balestra et al. (2007); (6) Smail et al. (2007).

**Table 2.** MACS medium-redshift ( $0.5 \leq z < 0.7$ ) sample

Cluster	RA (J2000)	Dec (J2000)	$z$	$L_X(0.1 - 2.4 \text{ keV})$ [ $10^{44} \text{ erg s}^{-1}$ ]	$M_{200}$ [ $10^{15} M_\odot$ ]	BCG $m_{F814W}$
MACSJ0018.5+1626	00:18:33.8	+16 : 26 : 16.6	0.546	19.6	3.3	19.6
MACSJ0025.4–1222	00:25:29.4	−12 : 22 : 37.1	0.584	8.8	1.8	—
MACSJ0257.1–2325	02:57:08.8	−23 : 26 : 03.3	0.505	13.7	2.5	18.3
MACSJ0454.1–0300	04:54:11.1	−03 : 00 : 53.8	0.538	16.8	2.9	18.9
MACSJ0647.7+7015	06:47:50.1	+70 : 14 : 56.4	0.591	15.9	2.8	18.9
MACSJ0717.5+3745	07:17:32.9	+37 : 45 : 05.4	0.546	24.6	3.9	—
MACSJ0744.8+3927	07:44:52.8	+39 : 27 : 26.7	0.698	22.9	3.7	19.1
MACSJ0911.2+1746	09:11:11.2	+17 : 46 : 34.8	0.505	7.8	1.6	18.8
MACSJ1149.5+2223	11:49:35.5	+22 : 24 : 04.2	0.544	17.6	3.0	18.9
MACSJ1423.8+2404	14:23:48.6	+24 : 04 : 49.1	0.543	16.5	2.9	18.1
MACSJ2129.4–0741	21:29:26.3	−07 : 41 : 26.2	0.589	15.7	2.6	19.5
MACSJ2214.9–1359	22:14:57.3	−14 : 00 : 12.2	0.503	14.1	2.5	18.2

Note - Redshifts and X-ray luminosities are from Ebeling et al. (2007).  $M_{200}$  are based on the  $L_X - M_{200}$  relation of Reiprich & Böhringer (2002). Last column gives the magnitude of the brightest cluster galaxy.

lit (ROSAT) All-Sky Survey (RASS, Voges et al. 1999), MACS covers  $22,735 \text{ deg}^2$  of extragalactic sky ( $|b| > 20 \text{ deg}$ ); the present MACS sample, estimated to be at least 90% complete, comprises 124 clusters all of which have spectroscopic redshifts. Owing to the high X-ray flux limit of the RASS and the lower redshift limit of  $z = 0.3$ , MACS clusters feature X-ray luminosities of, typically,  $5\text{--}10 \times 10^{44} \text{ erg s}^{-1}$  in the 0.1–2.4 keV band (Ebeling et al. 2007). MACS thus probes the high end of the cluster mass function, in-

cluding some of the most powerful gravitational lenses (Smith et al. 2009; Zitrin et al. 2009); see also Smail et al. (2007) for a spectacular case of galaxy-galaxy lensing in the field of a MACS cluster. MACS clusters have been used for a wide range of cosmological and astrophysical applications, e.g., in cosmological studies (Allen et al. 2008; Mantz et al. 2008, 2009a, b), investigations of large-scale structure (Ebeling, Barrett, & Donovan 2004; Kartaltepe et

al. 2008), and studies of the galaxy content and gas properties of individual clusters (e.g., Ma et al. 2008, 2009).

Here we use images of 35 MACS clusters observed with the ACS (GO-09722, GO-10491, GO-10875, PI Ebeling).

We divide these clusters into two subsamples according to redshift,  $0.3 \leq z < 0.5$ , and  $0.5 \leq z < 0.7$ , which consist of 23 and 12 clusters, respectively. The low-redshift sample was observed with *HST* in Snapshot mode, meaning the telescope schedulers chose a fraction of the targets from the full MACS sample, based solely on their scheduling convenience. Thus, the clusters we analyse are an unbiased, representative selection from the entire MACS sample. The medium-redshift sample consists of a complete set of 12 MACS clusters in this redshift range that are visible from Hawaii. Strong-lensing mass reconstructions of the clusters in this subsample have been recently presented by Zitrin et al. (2010).

The low-redshift clusters were observed through the F606W filter (mean wavelength  $\sim 6060$  Å) with exposure times of 1200 s, while the medium-redshift sample was observed through the F814W filter (mean wavelength  $\sim 8140$  Å) with exposure times of  $\sim 4500$  s. Applying the  $L_X - M_{200}$  relation<sup>1</sup> of Reiprich & Böhringer (2002) yields a cluster mass range of ( $1.4 \leq M_{200} \leq 4.1$ )  $\times 10^{15} M_\odot$ , and ( $1.6 \leq M_{200} \leq 3.9$ )  $\times 10^{15} M_\odot$  for the low- and medium-redshift samples, respectively. The cluster properties are listed in Tables 1 and 2.

## 2.2 X-ray Brightest Abell-type Clusters of galaxies (XBACs) $z \approx 0.2$ sample

The sample of Smith et al. (2005), as analyzed in H05, consists of 10 galaxy clusters from the X-ray Brightest Abell-type Clusters of galaxies (XBACs) catalogue (Ebeling et al. 1996), with  $0.17 < z < 0.26$ . The  $0.1 - 2.4$  keV flux limit of  $f_X \geq 5.0 \times 10^{-12}$  erg cm<sup>-2</sup> s<sup>-1</sup> applied to this redshift range implies X-ray luminosities  $L_X \geq 4.1 \times 10^{44}$  erg s<sup>-1</sup>, i.e. similar to the MACS clusters at their higher redshifts. Details of this sample and its properties can be found in table 1 of H05.

## 2.3 The Red-Sequence Cluster Survey (RCS)

The RCS survey was conducted using the Canada-France-Hawaii Telescope (CFHT) through the  $R_c$  and  $z'$  filters. Gladders & Yee (2005) applied a red-sequencing technique to an area of  $\sim 100$  deg<sup>2</sup>, and a catalogue of  $\sim 1000$  clusters at  $0.2 < z < 1.4$  was compiled. The survey is complete to  $5\sigma$  magnitude limits of 24.9 and 23.8 in  $z'$  and  $R_c$ , respectively. Like MACS clusters, RCS clusters have also been used in many applications, e.g., studying the scaling relations between different cluster properties (Hicks et al. 2008), and exploring the evolution of the red-sequence galaxy luminosity function (Gilbank et al. 2008).

Among the RCS clusters, a subset of 150 clusters was proposed for *HST* observation, again in Snapshot mode, out of which 52 were selected by *HST* schedulers based on scheduling convenience, and imaged using ACS, (GO-10626, PI Loh). Contrary to the MACS and XBACs clusters that we analyse here, which were chosen in an unbiased way from among complete samples, we do not know what were the criteria, if any, for selecting the 150 RCS clusters to be potential *HST* Snapshot targets. We suspect that there

**Table 3.** RCS low-redshift ( $0.3 \leq z < 0.5$ ) sample

Cluster	RA	Dec	$z$	BCG $m_{F814W}$
RCS022403-0227.7	02:24:03.4	-02 : 27 : 52.1	0.314	—
RCS035139-0956.4	03:51:39.5	-09 : 56 : 32.6	0.334	17.3
RCS044406-2820.5	04:44:06.4	-28 : 20 : 37.9	0.437	18.0
RCS051536-4325.5	05:15:37.0	-43 : 25 : 31.1	0.44	18.3
RCS051834-4325.1	05:18:35.2	-43 : 25 : 15.0	0.475	18.6
RCS092821+3646.5	09:28:22.3	+36 : 46 : 31.9	0.356	18.2
RCS110233-0319.2	11:02:33.5	-03 : 19 : 19.3	0.423	17.6
RCS110258-0521.2	11:02:59.2	-05 : 21 : 13.9	0.395	18.4
RCS110340-0458.1	11:03:40.7	-04 : 58 : 12.0	0.492	19.3
RCS131912-0206.9	13:19:12.7	-02 : 06 : 59.7	0.354	—
RCS145226+0834.6	14:52:27.3	+08 : 34 : 36.7	0.325	18.1
RCS145900.4+102336	14:59:00.8	+10 : 23 : 34.5	0.395	18.4
RCS151110.7+100203	15:11:11.1	+10 : 02 : 05.9	0.455	18.1
RCS151306.9+061124	15:13:06.5	+06 : 11 : 24.8	0.325	16.4
RCS211519-6309.5	21:15:20.3	-63 : 09 : 31.0	0.331	17.6
RCS212134-6335.8	21:21:35.0	-63 : 35 : 50.9	0.351	17.2
RCS215609.1+012319	21:56:09.3	+01 : 23 : 23.1	0.335	16.9
RCS223952-6044.8	22:39:52.8	-60 : 44 : 53.6	0.429	18.7

may have been some bias toward including clusters that already had evidence of strong lensing, based on previous ground-based imaging. However, it is highly unlikely that the 150 clusters were chosen, intentionally or unintentionally, in a way that would *avoid* systems with strong lensing (and it is also hard to imagine a logical reason for such a choice). The main result of our study will be that the RCS clusters observed by *HST* are inefficient as lenses, when compared to the truly unbiased sample of X-ray selected clusters. This conclusion, applied to the RCS clusters as a whole, will therefore only be strengthened, if the 150 RCS clusters were pre-selected to favor strong lenses. Our results will thus provide a firm and useful upper limit on the RCS lensing fraction.

The clusters were imaged through the F814W filter with exposure times of 1440 s. Luminosities and mass estimates of the RCS clusters have not been published to date. In §4 below, we show that the RCS clusters and the X-ray selected clusters above have similar optical luminosities.

As with the X-ray selected clusters above, we divide the RCS clusters into redshift bins: the same low ( $0.3 \leq z < 0.5$ ) and medium ( $0.5 \leq z < 0.7$ ) redshift subsamples which were defined above, and a third, high-redshift, subsample at  $0.7 \leq z \leq 1$ . The three redshift subsamples consist of 18, 18, and 16 clusters, respectively. The properties of the 52 RCS clusters are listed in Tables 3, 4, and 5.

## 2.4 Arc detection

In H05, we introduced the use of an automated arc detection algorithm to arc statistics studies. Automated arc detection is important for an objective, quantitative, and fair comparison of arc statistics in observed and simulated data. In the meantime, a number of other arc-detection algorithms have been published, by Lenzen et al. (2004), Alard (2006), and Seidel & Bartelmann (2007; SB07). In the present work, we subject all of the images to two of these algorithms, H05 and SB07.

The H05 arc-detection algorithm is based on application of the SExtractor (Bertin & Arnouts 1996) object identification soft-

<sup>1</sup>  $M_{200}$  is the mass enclosed within  $r_{200}$ , the radius within which the average density is equal to 200 times the critical cosmological density at the observed redshift.

**Table 4.** RCS medium-redshift ( $0.5 \leq z < 0.7$ ) sample

Cluster	RA	Dec	$z$	BCG $m_{F814W}$
RCS033414–2824.6	03:34:14.5	–28 : 24 : 34.5	0.668	—
RCS035027–0855.1	03:50:27.4	–08 : 55 : 13.5	0.584	19.0
RCS044207–2815.0	04:42:08.1	–28 : 15 : 11.3	0.522	18.9
RCS051128–4235.2	05:11:27.8	–42 : 35 : 11.6	0.518	18.3
RCS051855–4315.0	05:18:55.0	–43 : 15 : 00.9	0.544	19.0
RCS051919–4247.8	05:19:19.8	–42 : 47 : 49.2	0.603	19.9
RCS110104–0351.3	11:01:04.7	–03 : 51 : 21.3	0.639	—
RCS110733–0520.6	11:07:33.5	–05 : 20 : 39.4	0.597	18.7
RCS110752–0516.5	11:07:53.0	–05 : 16 : 35.0	0.579	19.4
RCS110814–0430.8	11:08:14.5	–04 : 30 : 53.9	0.638	—
RCS131722–0201.4	13:17:22.8	–02 : 01 : 28.8	0.535	18.2
RCS132335+3022.6	13:23:35.5	+30 : 22 : 43.7	0.538	18.1
RCS141910+5326.1	14:19:10.3	+53 : 26 : 07.5	0.647	19.4
RCS151840.1+084500	15:18:40.3	+08 : 45 : 05.0	0.515	18.7
RCS161547+3057.3	16:15:47.5	+30 : 57 : 14.1	0.514	18.8
RCS215223–0503.8	21:52:23.2	–05 : 03 : 44.2	0.545	18.7
RCS231654–0011.1	23:16:54.8	–00 : 11 : 06.8	0.56	19.6
RCS234717–3634.4	23:47:17.4	–36 : 34 : 32.6	0.537	18.8

**Table 5.** RCS high-redshift ( $0.7 \leq z \leq 1$ ) sample

Cluster	RA	Dec	$z$
RCS022453–0316.7	02:24:53.6	–03 : 16 : 47.5	0.906
RCS025242.5–150024	02:52:42.7	–15 : 00 : 28.0	0.995
RCS043934–2904.6	04:39:34.2	–29 : 04 : 43.9	0.786
RCS051940–4402.1	05:19:40.3	–44 : 02 : 13.8	0.913
RCS110439–0445.0	11:04:40.3	–04 : 45 : 03.2	0.715
RCS110651–0350.3	11:06:52.2	–03 : 50 : 23.8	0.768
RCS110723–0523.2	11:07:23.8	–05 : 23 : 16.1	0.794
RCS112225+2422.9	11:22:25.5	+24 : 22 : 51.3	0.799
RCS132939+2853.3	13:29:39.8	+28 : 53 : 14.3	0.901
RCS145039+0840.7	14:50:40.2	+08 : 40 : 46.9	0.769
RCS162009+2929.4	16:20:09.2	+29 : 29 : 33.8	0.797
RCS211852–6334.6	21:18:52.6	–63 : 34 : 43.1	0.786
RCS212238–6146.1	21:22:38.3	–61 : 46 : 17.0	0.856
RCS215248–0609.4	21:52:49.2	–06 : 09 : 24.4	0.704
RCS231831+0034.3	23:18:31.8	+00 : 34 : 22.8	0.809
RCS234220–3534.3	23:42:20.4	–35 : 34 : 15.5	0.802

ware. The output of repeated SExtractor calls, using different detection parameters each time, is filtered using some threshold of object elongation. The final SExtractor call is executed on an image combined from the filtered “segmentation image” outputs of the previous calls. The arc candidates detected in that last call are included in the final arc catalogue if they meet the required detection parameters defined by the user.

The SB07 algorithm is based on light moments. The image is divided into small cells which are iteratively moved to their local light centres. Then, for each cell, an ellipticity vector is calculated using light moments. Adjacent cells with similarly oriented ellipticity vectors are joined together and considered as part of an arc candidate, whose outer boundary is determined by an active con-

tour method. Candidates are accepted if they conform to specified parameters.

In the present work, we apply an acceptance criterion on arc length-to-width ratio of  $l/w \geq 8$ . We also use a magnitude limit of  $m \leq 24$  as another acceptance criterion which, given the exposure times of our sample, results in the detection of arcs with signal-to-noise  $S/N \gtrsim 3$ . Our magnitude limit is higher than most of the magnitude limits used in previous studies, such as B98 and Zaritsky & Gonzales 2003, allowing us to include fainter arcs in our analysis. Nevertheless, our acceptance threshold for arc detections is brighter than the arc detection limits of all the images, with their range of exposure times and filters, thus permitting a meaningful comparison of arc statistics among the various subsamples. This holds also for the WFPC2 images of the XBACS sample. Although WFPC2 was less sensitive than ACS, the WFPC2 exposure times were longer, typically 7000 s, leading to similar depths. Furthermore, the somewhat lower angular resolution of WFPC2, due to its larger pixels ( $0''.1$ ), is not important, since the arcs we consider are always much larger, and all the arcs we find below in ACS images would have been detected in long WFPC2 exposures as well. We note that we use total-magnitude limit for arcs, rather than considering surface brightness, which could also plausibly be used. We do this to conform with previous observational and theoretical studies, but also because arcs, especially at HST resolution, display rich structure and unresolved clumps, and hence it is not clear that mean surface brightness would be a more relevant observable. Due to the varying position of the cluster centres within the FOV, the cluster coverage area varies. We therefore also limit our search to a  $60''$  radius from the cluster centre. The automated arc detection results were visually inspected in order to remove false positives such as spikes from saturated stars, galaxy spiral arms, and edge-on galaxies.

While most of the arcs in our sample are detected by both programs, a few unmistakable lensed arcs are picked out by only one or the other. The SB07 arcfinder is more successful than the H05 arcfinder in detecting arcs that are superimposed on the light of cluster galaxies. On the other hand, the H05 arcfinder produce a better “segmentation” compared to the SB07 arcfinder, which sometimes breaks arcs into smaller arclets, which then do not qualify as giant arcs. We defer a more detailed comparison of these and other arcfinders to a future study.

### 3 RESULTS

Figure 1 shows the ACS images of the clusters in which arcs are detected, and Figure 2 provides zoom-ins on the individual arc features. Table 6 lists the properties of the detected arcs, which we discuss in more detail below.

#### 3.1 X-ray selected clusters

In the MACS sample we identify a total of 26 arcs in 12 out of the 23 low-redshift clusters, and a total of 16 arcs in 9 out of the 12 medium-redshift clusters. All but 3 of these arcs (in two clusters) have not been previously reported (see Table 6). The arcs span a magnitude range of  $20 < m < 24$  and a  $l/w$  ratio range of  $8 - 29$ . As shown in Figure 3, over half of the cluster lenses, in both the low- and medium-redshift MACS subsamples, produce multiple arcs. A similar result was found in the XBACS sample of H05, in which 17 arcs (with  $l/w \geq 8$ ), in 7 out of the 10 clusters at  $z \approx 0.2$ , were detected.

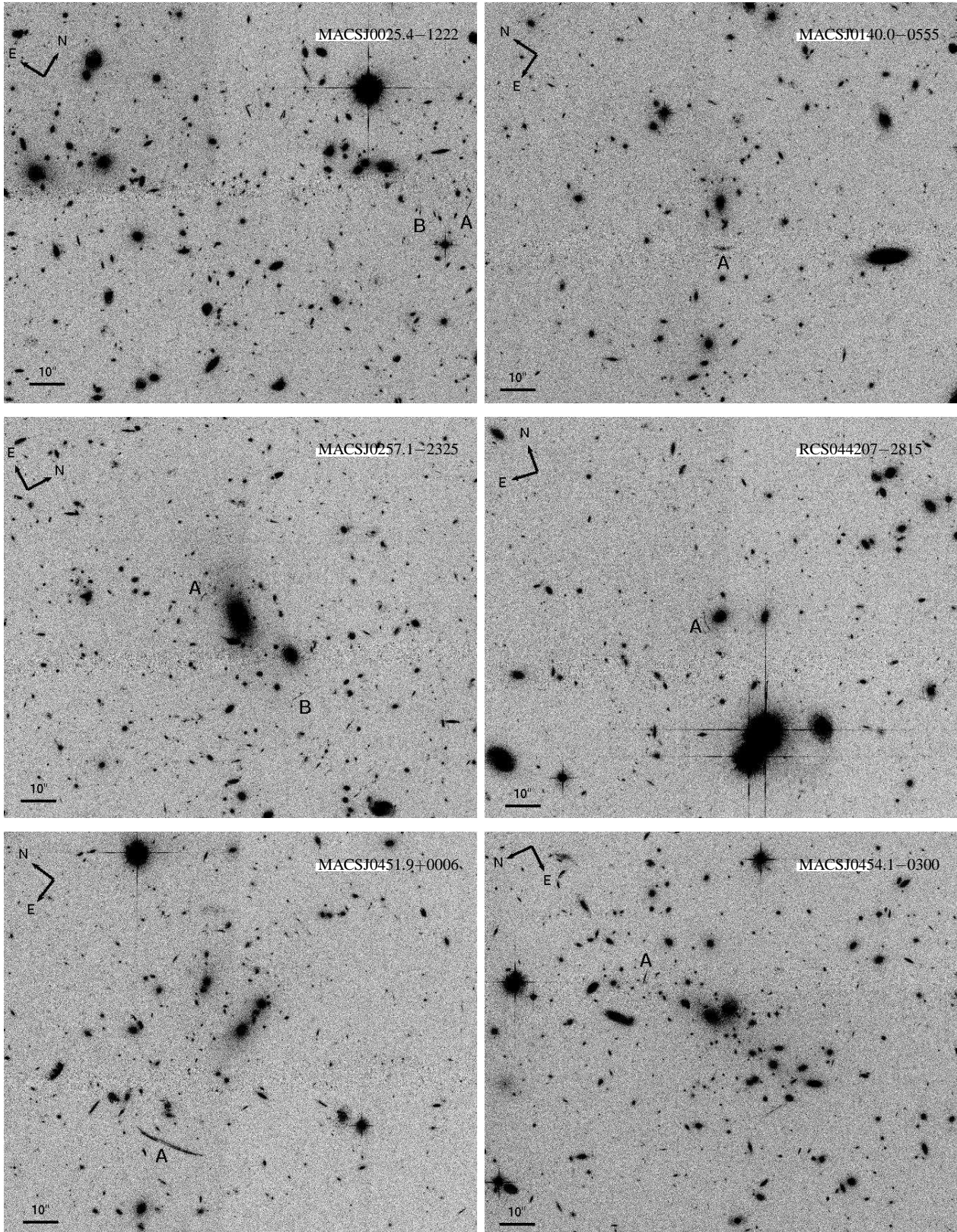


**Figure 1.**  $2\frac{1}{2} \times 1\frac{1}{9}$  sections of the HST/ACS images of the clusters, showing the location of detected arcs. See Fig. 2 for a detailed view of each arc.

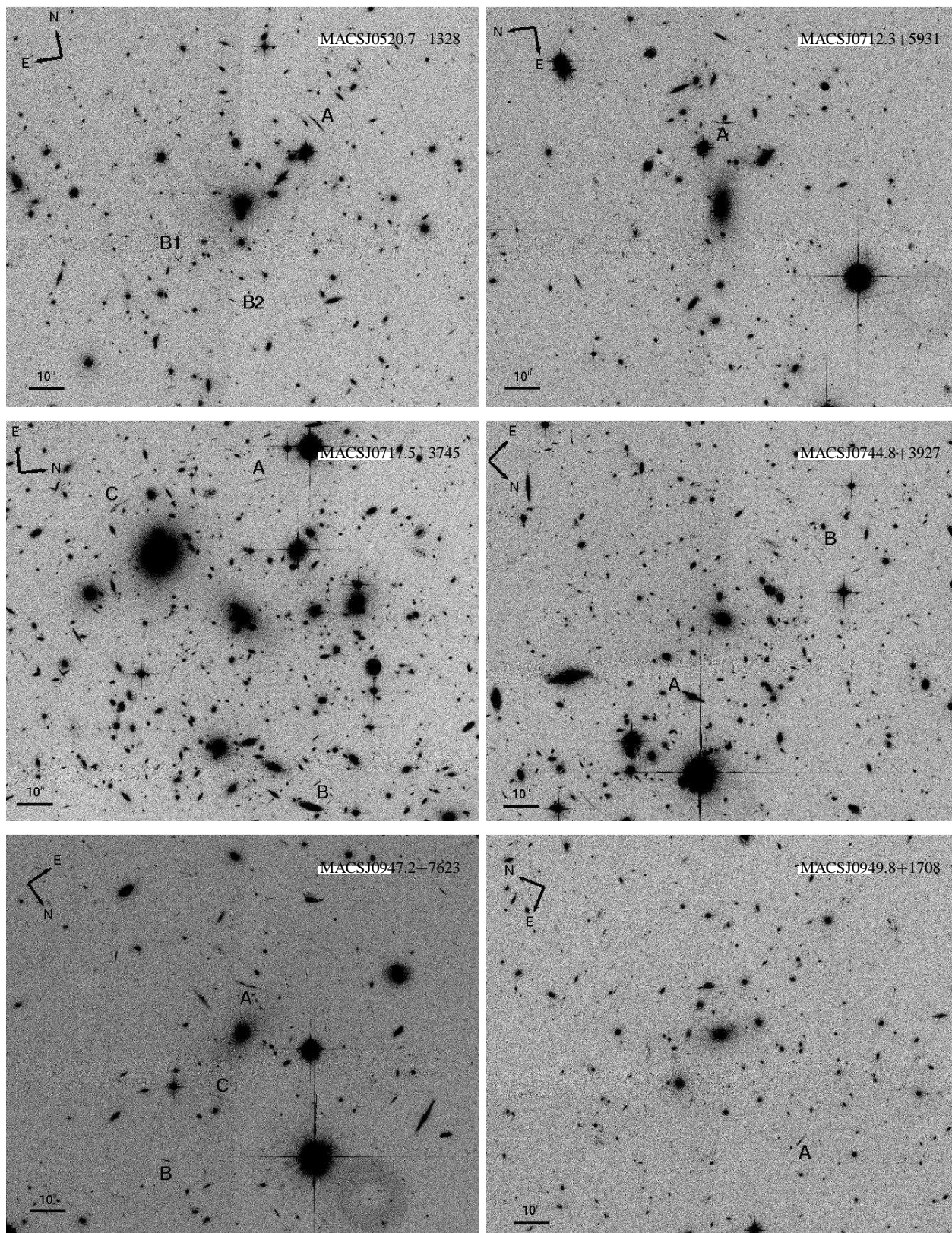


**Figure 1.** [continued]

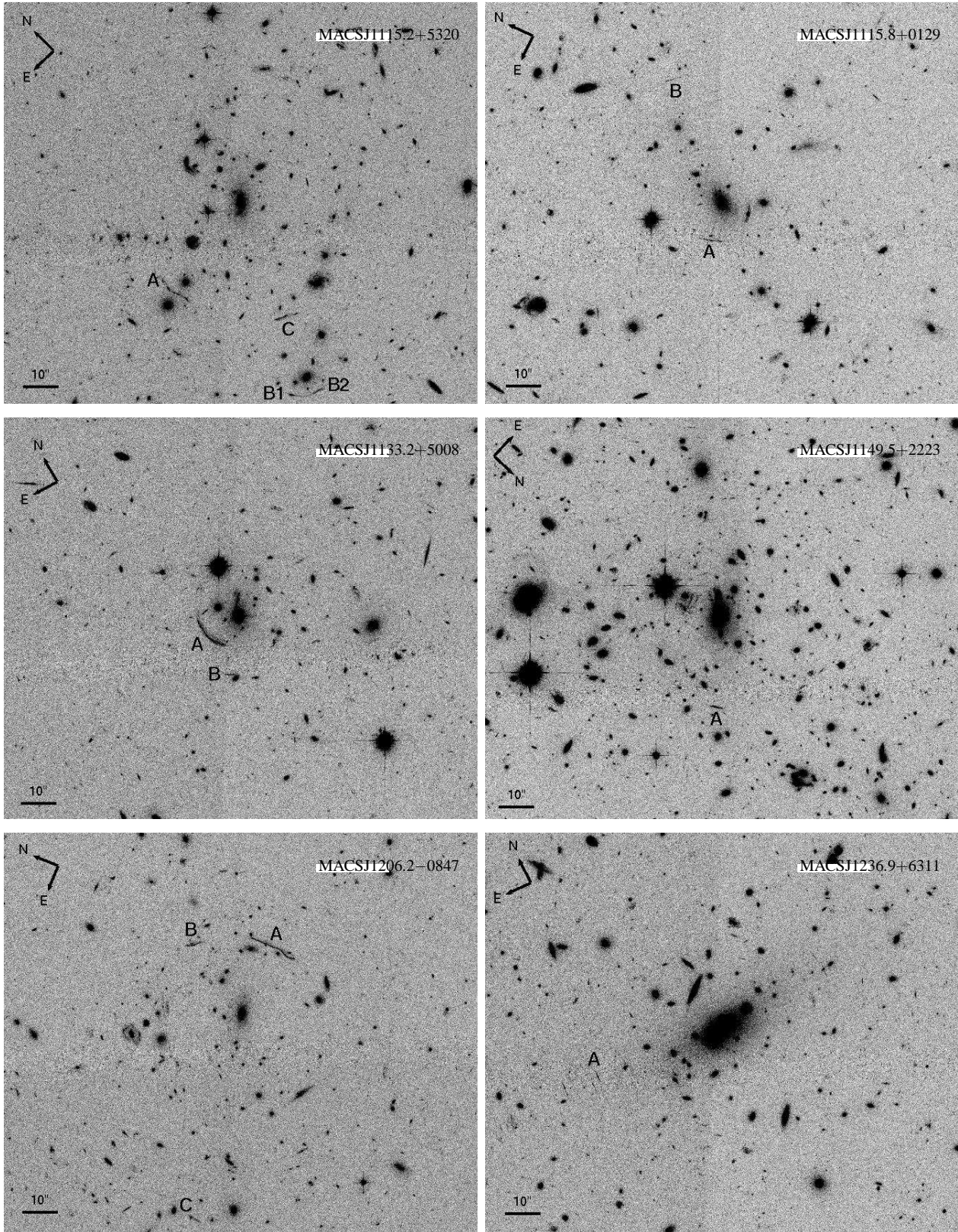


Figure 1. [continued]

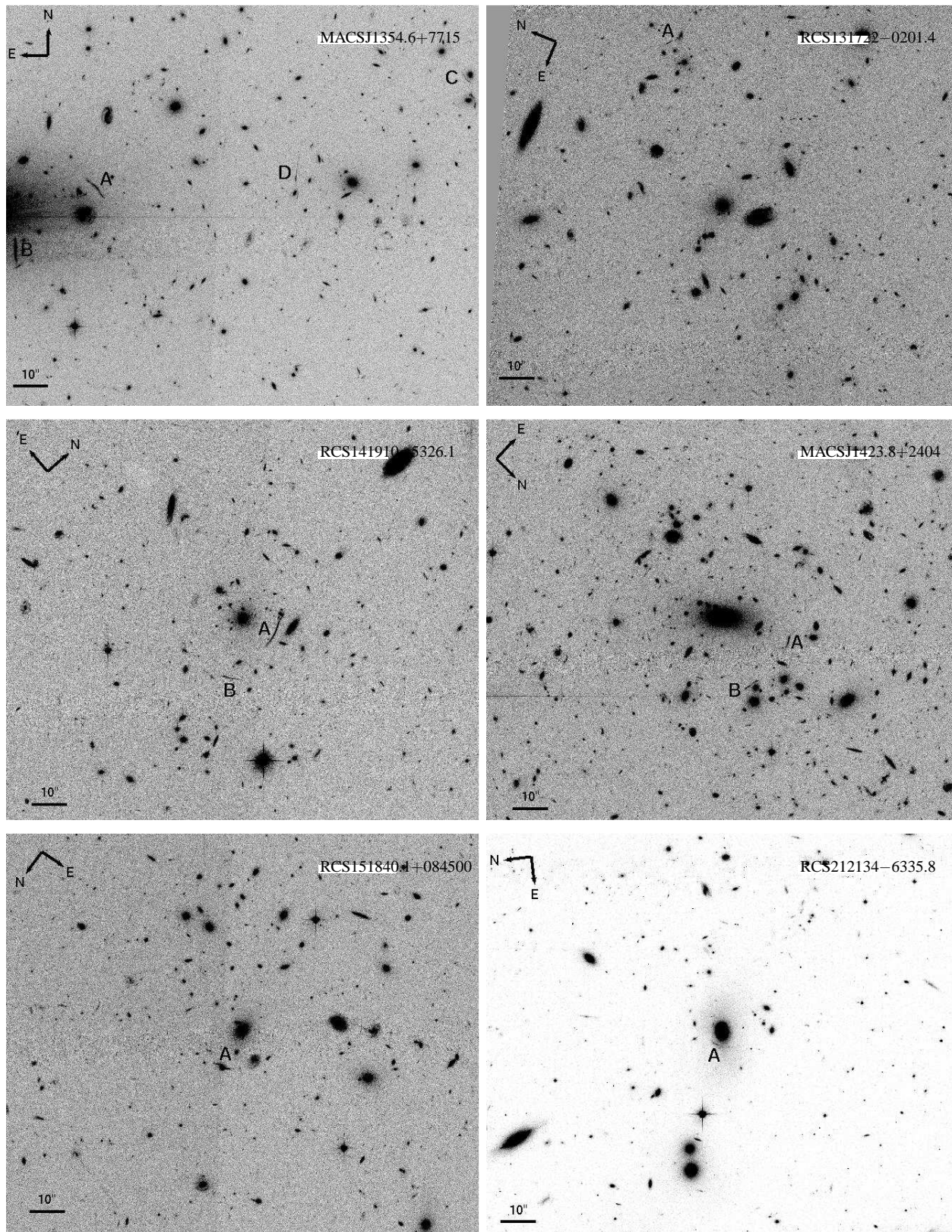


Figure 1. [continued]

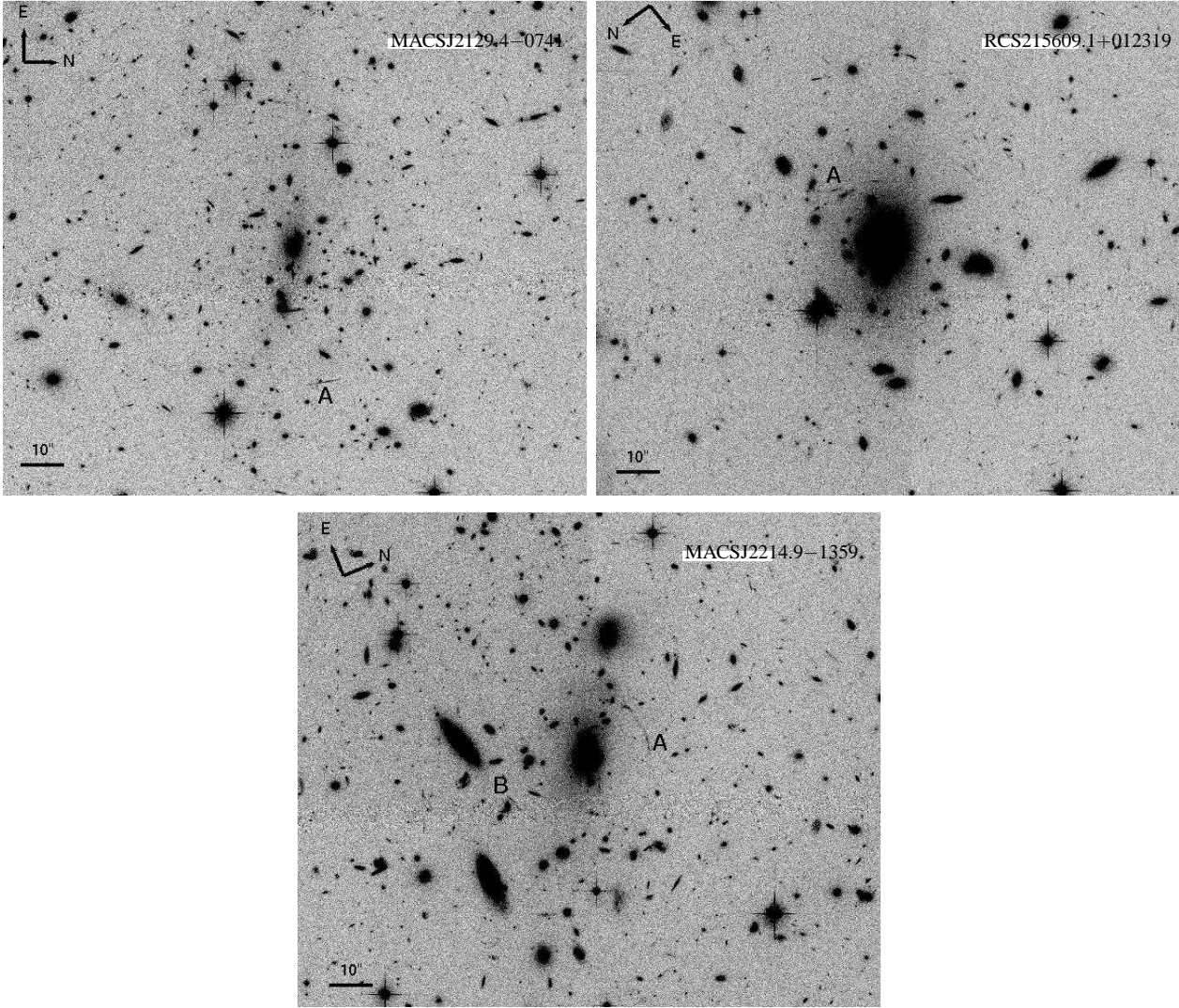


Figure 1. [continued]

In terms of the distribution of the angular separation of arcs from the cluster centres, in the low-redshift MACS subsample, as shown in Fig. 4, the lensed arcs are uniformly distributed at separation angles of  $10'' - 50''$ . In the medium-redshift MACS sample, the arcs are distributed slightly closer to the cluster centres, but both distributions are consistent, given the small numbers per bin. There are no arcs in this sample beyond  $35''$ . Since there is an uncertainty concerning the centre position of the cluster MACSJ1354.6+7715, as discussed below, we do not include its arcs in the above analysis. In addition, each of the apparently merging arc pairs MACSJ0520.7-1328 B1/B2 and MACSJ1115.2+5320 B1/B2, are treated as one arc. We also exclude the arcs in MACSJ0717.5+3745 from this analysis, since this cluster is highly disturbed (Ma, Ebeling, & Barrett; 2009) and therefore its centre cannot be easily determined.

### 3.2 Optically selected clusters

Only two arcs are detected in the low-redshift RCS cluster subsample. While both arcs have  $l/w \geq 10$ , they are still relatively short ( $< 5''$ ) compared to some of the arcs found in the MACS sample,

which can be as long as  $20''$ . In the medium-redshift optical subsample, 5 arcs are found in 4 out of the 18 clusters. Two of these arcs (in one cluster, see Table 6) have been previously reported. No arcs are detected among the 16 clusters of the high-redshift ( $0.7 \leq z \leq 1$ ) optical subsample.

As seen in Fig. 4 and Table 6, compared to the X-ray sample, the arcs in the RCS sample occur at significantly smaller separations, generally  $< 20''$ , and sometimes only  $3 - 5''$ . The only exception is RCS131722-0201.4, whose arc appears  $48''$  from the cluster centre. However, as seen in Figs. 1 and 2, this arc may actually be a small-separation image produced by the local mass concentration traced by the galaxies near the arc. Since arcs occur near critical curves, the small separations suggest significantly smaller Einstein radii, and hence masses, for the RCS clusters.

### 3.3 Arc production efficiency

Table 7 summarizes the arc statistics of our various cluster subsamples. As noted above, only two arcs are detected in the RCS low-redshift subsample, compared to the 26 arcs detected in the low-redshift MACS subsample. The arc production efficiencies are,

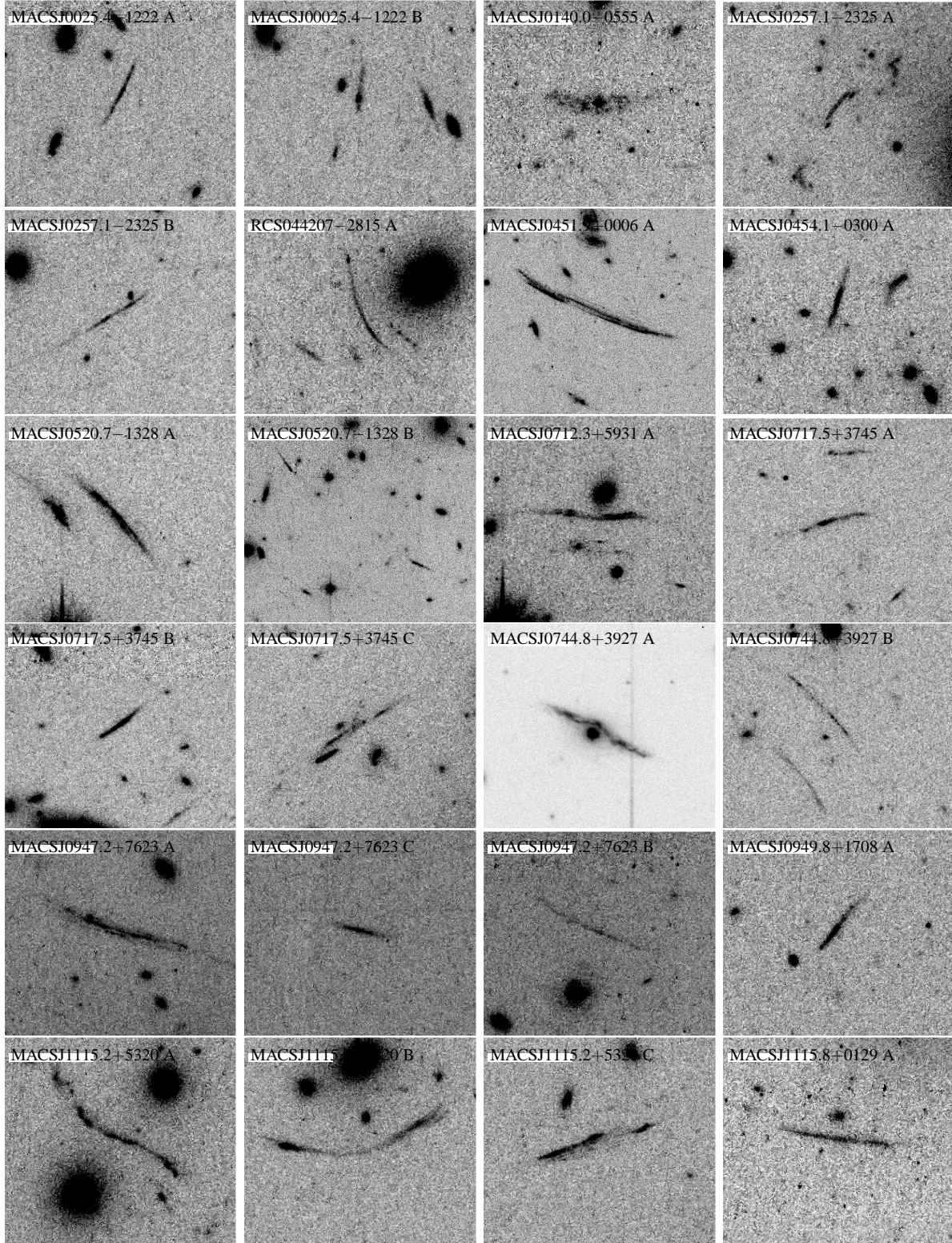


**Figure 2.** Arcs detected in our sample. Each frame is a  $14'' \times 12''$  section of the HST/ACS image. The frame of MACS0451.9+0006 A is a  $28'' \times 24''$  image section. Orientations are as in Fig. 1.

**Table 6.** Detected arcs and properties

Cluster	Arc ID	Length [arcsec]	Width [arcsec]	$l/w$	$m_{F606W}/$ $m_{F814W}$ [mag]	Radial separation from cluster centre [arcsec]
MACSJ0025.4–1222	A	3.3	0.2	13.9	23.6	—
	B	2.7	0.3	9.64	23.7	—
MACSJ0140.0–0555	A	5.1	0.6	8.3	21.8	13.7
MACSJ0257.1–2325	A	3.0	0.3	10.6	23.7	11.6
	B	3.5	2.8	12.7	23.5	27.8
RCS044207–2815.0	A	4.3	0.2	18.5	23.0	4.5
MACSJ0451.9+0006	A	20.2	0.7	29.3	20.5	38.3
MACSJ0454.1–0300	A	3.7	0.4	10.4	22.3	21.8
MACSJ0520.7–1328	A	6.1	0.5	12.2	22.2	30.9
	B1	2.3	0.3	8.6	23.7	24.1
	B2	2.6	0.3	8.8	23.5	27.4
MACSJ0712.3+5931	A	5.2	0.3	17.9	22.8	23.2
MACSJ0717.5+3745	A	4.2	0.3	15.4	23.0	—
	B	3.0	0.4	8.5	22.7	—
	C	4.6	0.2	19.0	23.1	—
MACSJ0744.8+3927	A	6.1	0.5	12.3	20.5	23.3
	B	5.1	0.2	27.3	23.9	35.0
MACSJ0947.2+7623	A	6.4	0.4	14.3	22.3	13.5
	B	2.9	0.3	14.7	22.6	41.7
	C	6.5	0.3	23.0	23.4	19.1
MACSJ0949.8+1708	A	3.3	0.4	8.8	22.8	37.6
MACSJ1115.2+5320	A	3.2	0.3	10.2	23.6	31.6
	B1	3.4	0.3	10.3	22.9	56.2
	B2	3.5	0.4	8.5	23.5	57.3
	C	4.4	0.5	8.5	22.3	34.5
MACSJ1115.8+0129	A <sup>1</sup>	4.8	0.3	15.1	23.2	11.2
	B	5.1	0.2	26.7	23.7	37.2
MACSJ1133.2+5008	A	11.7	0.8	14.6	21.0	10.5
	B	2.5	0.2	10.2	23.5	17.0
MACSJ1149.5+2223	A	4.0	0.5	8.4	22.2	26.0
MACSJ1206.2–0847	A <sup>2</sup>	13.9	0.5	26.8	21.1	20.7
	B <sup>2</sup>	4.8	0.5	8.8	22.4	23.8
	C	3.7	0.5	8.2	23.3	59.3
MACSJ1236.9+6311	A	2.9	0.3	10.6	23.8	38.0
MACSJ1354.6+7715	A	7.7	0.6	12.9	21.7	—
	B	7.6	0.9	8.8	21.1	—
	C	3.4	0.2	14.6	23.8	—
	D	4.6	0.3	17.6	23.4	—
RCS131722–0201.4	A	2.6	0.3	10.1	23.0	48.4
RCS141910+5326.1	A <sup>3</sup>	10.5	0.6	17.3	20.2	10.0
	B <sup>3</sup>	3.8	0.3	11.3	22.4	17.2
MACSJ1423.8+2404	A	4.2	0.4	10.3	22.7	19.7
	B	3.6	0.2	14.5	23.3	20.6
RCS151840.1+084500	A	3.8	0.3	11.9	21.6	11.2
RCS212134–6335.8	A	3.8	0.4	10.4	21.6	3.4
MACSJ2129.4–0741	A	5.4	0.3	17.3	22.1	31.5
RCS215609.1+012319	A	3.7	0.3	11.2	22.8	18.3
MACSJ2214.9–1359	A	4.0	0.3	12.4	23.3	14.3
	B	4.9	0.3	17.9	23.0	20.1

Notes: Arcs previously reported by: <sup>1</sup>Sand et al. (2005); <sup>2</sup>Ebeling et al. (2009); <sup>3</sup>Gladders et al. (2003).

therefore,  $0.11^{+0.15}_{-0.07}$ , and  $1.13^{+0.27}_{-0.22}$  arcs per cluster for the RCS and MACS subsamples, respectively, where we cite a 68% confidence interval assuming Poisson statistics. In the medium-redshift bin, the MACS clusters are also more efficient lenses than the RCS clusters, with efficiencies of  $1.33^{+0.42}_{-0.33}$ , and  $0.28^{+0.19}_{-0.12}$  arcs per cluster, respectively.

With zero detected arcs, the high-redshift RCS sample has an arc production efficiency of  $< 0.24$  arcs per cluster (95% confidence), which is consistent with the RCS efficiencies at lower  $z$ . As the arc occurrence frequency is consistent among different redshift bins, we tabulate also the total frequency in the X-ray versus the optical subsamples. The frequencies differ at the  $5\sigma$  level.

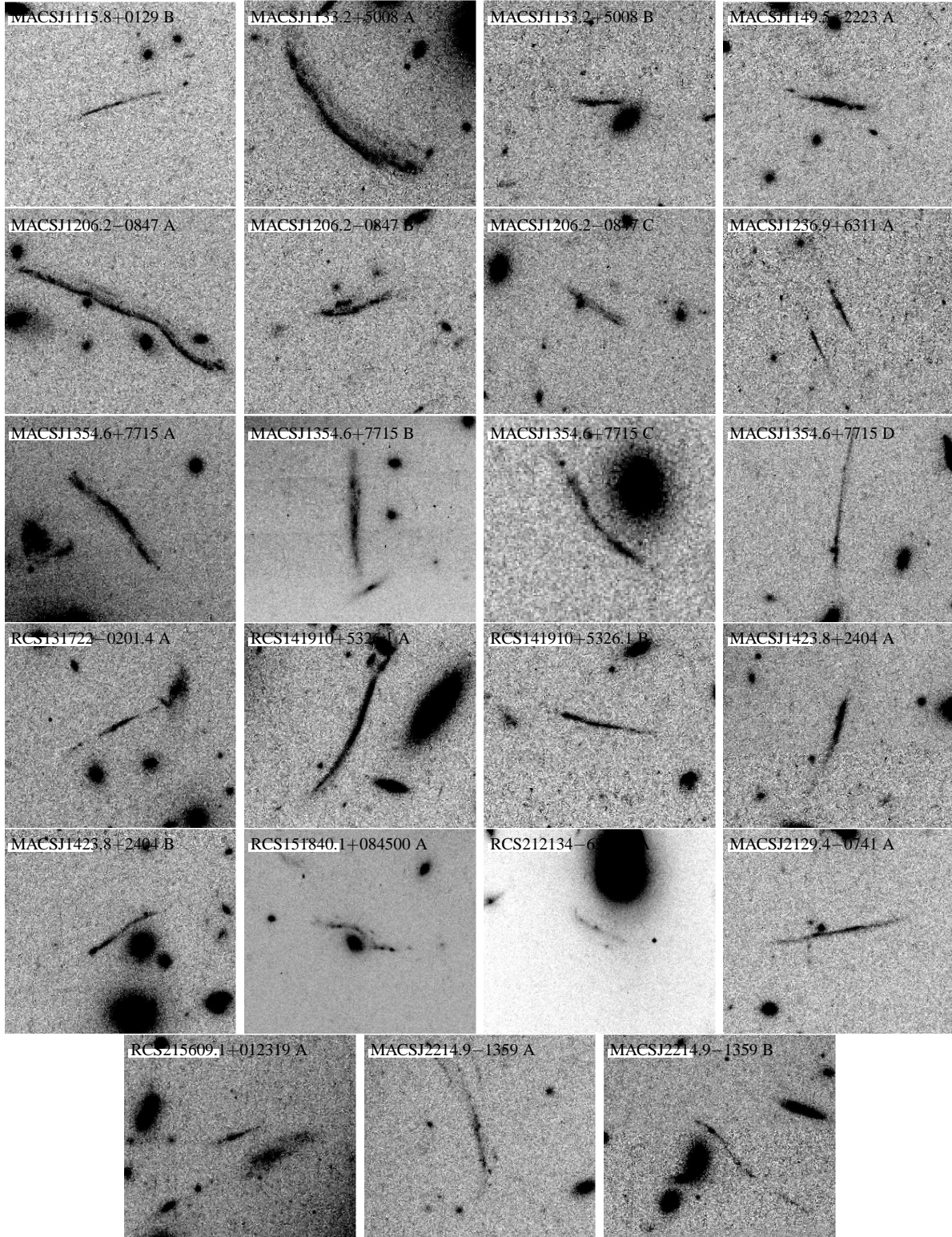
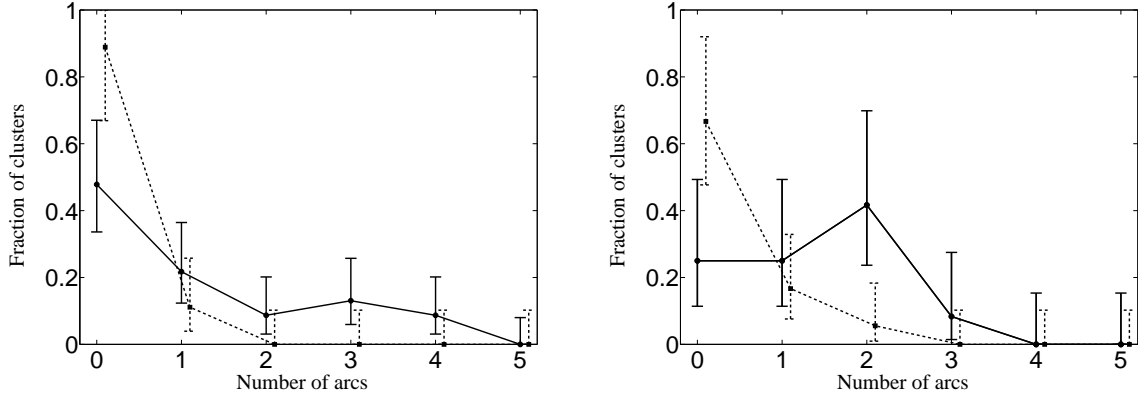


Figure 2. [Continued]

We also derive the arc production efficiencies for arcs with  $l/w \geq 10$ , for comparison with previous studies in which this  $l/w$  ratio was used to define giant arcs. All of the RCS arcs have  $l/w \geq 10$  and therefore the RCS cluster efficiencies remain unchanged. However, the MACS cluster production efficiencies of arcs with

$l/w \geq 10$  are somewhat lowered to  $0.74^{+0.23}_{-0.18}$ , and  $1.08^{+0.39}_{-0.23}$  arcs per cluster for the low-, and medium-redshift subsamples, respectively. Even so, both the low- and medium-redshift MACS clusters are significantly more efficient lenses ( $> 3\sigma$ ) than their RCS counterparts.



**Figure 3.** Distributions of the MACS (solid line) and RCS (dashed line) clusters as a function the number of arcs in an individual cluster. Left panel is the low-redshift subsample. Right panel is the medium-redshift subsample.

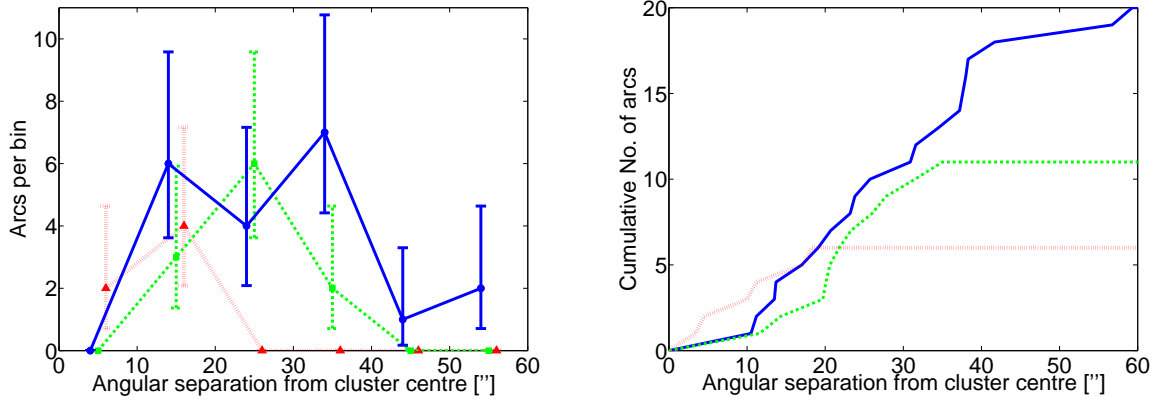


**Figure 4.** Distribution of arc angular separations from cluster centres in various subsamples. Left panel is the binned distribution, right panel is cumulative. Solid (blue) line is the low-redshift MACS subsample, dashed (green) line is the medium-redshift MACS subsample, and dotted (red) line is the RCS sample (all redshifts combined). For clarity, error bars are omitted for bins with zero arcs. We have also omitted the arc in RCS131722–0201.4, which is 48'' from the centre of the cluster, as it is likely associated with a local mass concentration near the arc rather than with the whole cluster.

**Table 7.** Arc statistics summary

Subsample	$N_{clusters}$	$N_{lenses}$	$N_{arcs}$		Arcs per cluster	
			$(l/w \geq 8)$	$(l/w \geq 10)$	$(l/w \geq 8)$	$(l/w \geq 10)$
X-ray selected clusters						
XBACs ( $0.17 \leq z \leq 0.26$ )	10	7	17	12	$1.7^{+0.52}_{-0.41}$	$1.2^{+0.46}_{-0.34}$
MACS ( $0.3 \leq z < 0.5$ )	23	12	26	17	$1.13^{+0.27}_{-0.22}$	$0.74^{+0.23}_{-0.18}$
MACS ( $0.5 \leq z < 0.7$ )	12	9	16	13	$1.33^{+0.42}_{-0.33}$	$1.08^{+0.39}_{-0.23}$
MACS ( $0.3 \leq z < 0.7$ )	35	21	42	30	$1.20^{+0.22}_{-0.18}$	$0.86^{+0.19}_{-0.16}$
Total ( $0.17 \leq z < 0.7$ )	45	28	59	42	$1.31^{+0.19}_{-0.17}$	$0.93^{+0.17}_{-0.14}$
Optically selected clusters						
RCS ( $0.3 \leq z < 0.5$ )	18	2	2	2	$0.11^{+0.15}_{-0.07}$	$0.11^{+0.15}_{-0.07}$
RCS ( $0.5 \leq z < 0.7$ )	18	4	5	5	$0.28^{+0.19}_{-0.12}$	$0.28^{+0.19}_{-0.12}$
RCS ( $0.7 \leq z \leq 1$ )	16	0	0	0	$0^{+0.12}_{-0}$	$0^{+0.12}_{-0}$
RCS ( $0.3 \leq z < 0.7$ )	36	6	7	7	$0.19^{+0.10}_{-0.07}$	$0.19^{+0.10}_{-0.07}$
Total ( $0.3 \leq z \leq 1$ )	52	6	7	7	$0.13^{+0.07}_{-0.05}$	$0.13^{+0.07}_{-0.05}$

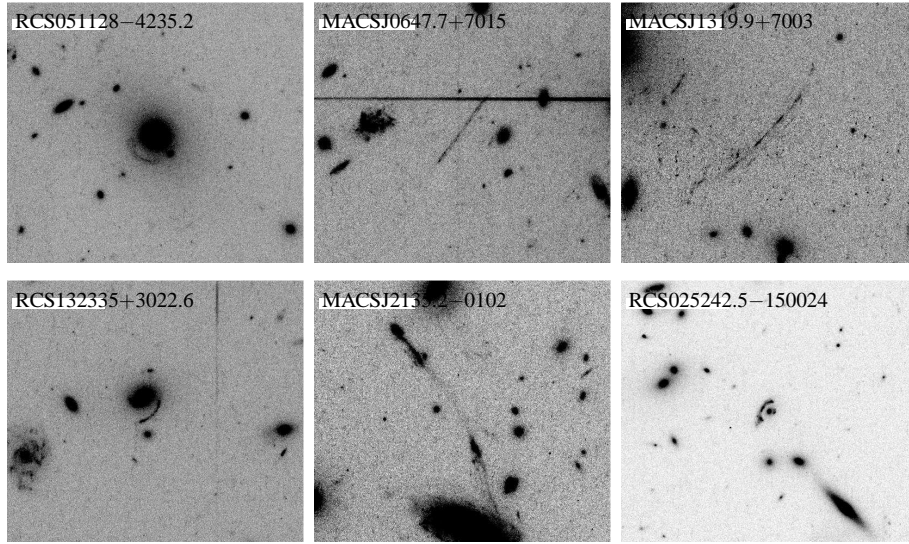


**Figure 5.**  $28'' \times 24''$  image section of arcs which were not detected algorithmically, using our detection thresholds, and therefore not included in our arc catalogue.

### 3.4 Notes on individual objects

#### 3.4.1 Lensing signatures in clusters without giant arcs

In addition to the automatic detection results, we have visually inspected all of the clusters in our sample. We find that there are several clusters that show signs of strong lensing but in which no arc was detected algorithmically, using our detection thresholds. In some cases, the arcs are too faint, while in others the arcs may be bright but have a length-to-width ratio below our threshold. Sometimes, an arc is projected close to another galaxy, making its detection difficult. We find six such clusters with signatures of strong lensing that are not included in our arc catalogue. Two of the clusters (MACSJ1319.9+7003 and MACSJ2135.2-0102), are found in the low-redshift MACS subsample, two (RCS051128-4235.2 and RCS132335+3022.6) are in the medium-redshift RCS subsample, the fifth cluster, MACSJ0647.7+7015, is in the medium-redshift MACS subsample, and the sixth cluster, RCS RCS025242.5-150024, is in the high-redshift RCS subsample. Figure 5 shows each of these cases.

#### 3.4.2 MACSJ1354.6+7715 - another bullet cluster ?

Inspection of the image of MACSJ1354.6+7715 suggests the existence of two separate galaxy concentrations. Arcs A and B (see Fig. 1) seem to straddle one centre. About  $75''$  west of that centre there seems to be another mass concentration enclosed by arcs C and D. We note that south of arc C there is an additional arc which is not included in our arc catalogue due to its small  $l/w$  ratio. The two galaxies at the centres of the two concentrations have magnitudes of 19.8 mag (east clump), and 19.2 mag (west clump). This cluster may be during some stage of a merger, but with still a considerable amount of substructure. Although the two clumps may be chance projections of two clusters at different redshifts, this is unlikely given the rarity of such massive lensing clusters. Moreover, the optical colors of the early-type galaxies across the field are also consistent with a single redshift. Existing ROSAT data show that the X-ray emission is centred on the system, but the entire HST/ACS field shown in Fig. 6 spans only a few ROSAT resolution elements, making it impossible to say anything about

the X-ray flux distribution relative to the two mass and optical-light concentrations. Higher resolution X-ray imaging (already approved with *Chandra*) and optical spectroscopy are needed to select among these alternatives.

#### 3.4.3 Radial arcs in MACSJ2129.4-0741 ?

Close inspection of the central area of the cluster MACSJ2129.4-0741 reveals two objects that appear to be radially distorted (See Fig. 7). The image parity of each of these objects seems to be flipped, as expected in lensing. An alternative explanation for these objects is tidal tails due to physical interaction between galaxies. Again, optical spectroscopy is needed to resolve the issue.

#### 3.4.4 A large arc in the field of the high redshift cluster RCS025242.5-150024.

We have found an extraordinarily large arc ( $10''$ ) in the cluster RCS025242.5-150024 (Fig. 8). This arc is found near a galaxy which is too bright ( $m_{F814W} = 17.8$ ) to belong to this high redshift ( $z = 0.995$ ) cluster. It seems that the arc is produced by the gravitational field of this foreground galaxy, and therefore we do not include it in our arc catalogue.

## 4 DISCUSSION

The results of our arc survey, presented above, can serve as a new and improved observational basis for future arc statistic studies. However, our survey also shows clearly that the arc-production efficiency of X-ray-selected clusters such as MACS and XBACS is higher by a factor of 5 – 10 than that of RCS clusters. In this section, we carry out additional analysis and discussion of the meaning of this result.

At a given redshift, the cross section for lensed arc formation depends primarily on mass, although mass profile, ellipticity and substructure are also important. The mass dependence weakens towards the high mass end at  $M_{200} \sim 10^{15} M_{\odot}$  (Dalal et al.



**Figure 6.** A  $195'' \times 105''$  image section (north is up) of the cluster MACSJ1354.6+7715. The color (in electronic version) image is a composite of the F606W and F814W HST/ACS images. The conspicuous feature on the left side is scattered light from a bright star outside the field of view.

2004; Hennawi et al. 2007). The stark difference in the arc frequency between the X-ray selected and optically selected clusters immediately raises the possibility that they probe different mass ranges. Based on their X-ray luminosities, the X-ray selected clusters have masses of  $M_{200} > 10^{15} M_{\odot}$ . Unfortunately, there is scant information of the X-ray properties of the RCS clusters, and hence on their masses. For example, Hicks et al. (2008) recently observed with *Chandra* a sample of 13 RCS clusters, of which detailed analysis was possible for nine. They found significant differences in the mass-temperature-luminosity relations of X-ray selected and RCS clusters, X-ray underluminosity in some RCS clusters, and evidence that RCS clusters have a larger fraction of their baryons in stars. Nevertheless, since optical flux is one of the few observables we do have available for the RCS clusters, we begin by comparing the optical luminosities of the MACS and RCS subsamples. The HST/ACS field of view covers only the central core regions of the clusters, and therefore we examine several proxies for the optical luminosity.

As a first proxy for optical luminosity, we examine the luminosities of the brightest cluster galaxies (BCGs) of the RCS and MACS samples. In SDSS clusters, Hansen et al. (2005) have found a correlation between cluster mass and BCG luminosity. The BCG magnitudes were measured using SExtractor by including the light from pixels which belong to the BCG and are above the detection threshold. Since the low-redshift subsamples are observed through different filters, we first calculate the F606W–F814W color for each RCS cluster redshift using an elliptical galaxy spectral template from Kinney et al. (1996), and convert the RCS cluster BCG F814W magnitudes to F606W. In this comparison we exclude the following clusters (four MACS and five RCS) due to the uncertainty in determining their centres and in identifying the dominant BCGs: MACSJ0916.1–0023, MACSJ1354.6+7715, MACSJ2243.3–0935, MACSJ0257.1–2325, RCS131912–0206.9, RCS022403–0227.7, RCS110104–0351.3, RCS033414–2824.6, and RCS110814–0430.8.

We find that the BCG magnitudes are more uniformly distributed in the RCS subsample than in the MACS subsample, and the BCGs span a wider magnitude range. Nevertheless, in

the low-redshift MACS and RCS subsamples, the median BCG absolute magnitudes are,  $M_{606} = -21.9$  and  $M_{606} = -22$ , respectively. Likewise, in the the medium-redshift MACS and RCS subsamples the median BCG magnitudes are  $M_{814} = -23.8$ , and  $M_{814} = -23.6$ , respectively. A Kolmogorov-Smirnov (KS) test indicates that for both the low- and the medium-redshift subsamples, the null hypothesis that both the RCS and MACS BCG magnitudes are derived from the same parent distribution cannot be confidently rejected (probabilities of 0.12 and 0.35, respectively, for the null hypothesis). These numbers are summarized in Table 8.

For a second comparison of optical luminosities, we measure integrated optical luminosity of the brightest galaxies within the cluster cores. We measure the total light of galaxies inside a physical aperture of radius 270 kpc (at low  $z$ ) and 370 kpc (at medium  $z$ ). The contribution of foreground and background galaxies to the light is determined statistically in annuli of 400–530 kpc and 550–730 kpc, for the low- and medium-redshift subsamples, respectively, and subtracted from the core light. The area in which we measure the “background” is still well within the cluster, and hence, our cluster core luminosities are underestimated due to background over-subtraction. Nevertheless, barring large profile differences (see below), these biased estimates of cluster luminosity can still be compared meaningfully between the X-ray and optical samples. We include only the light from objects with magnitudes fainter than the cluster BCG magnitude, but brighter than 24 mag. We convert the MACS low-redshift subsample’s F606W luminosities to F814W luminosities assuming, again, the Kinney et al. (1996) elliptical galaxy template and the filter transmission curves for the two bands. The resultant optical luminosity distributions (Fig. 9) of both the RCS and MACS cluster are consistent with being drawn from the same parent distribution (0.12 and 0.37 probabilities for the null hypothesis, see Table 8).

Finally, as a third method of comparing optical luminosities, we simply count the light from **all** the pixels inside the above apertures and annuli (but still leaving out the light from objects brighter than the BCG). This method takes into account the light from all the stars in the cluster cores, including stars in galaxies below the detection limit and diffuse intracluster light. As in the previous

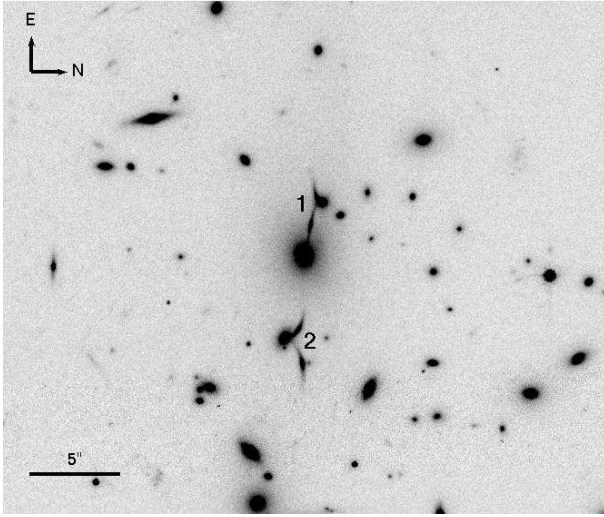


**Figure 7.**  $33'' \times 28''$  image sections of two radially distorted objects (marked as 1 and 2) in the cluster MACSJ2129.4-0741.

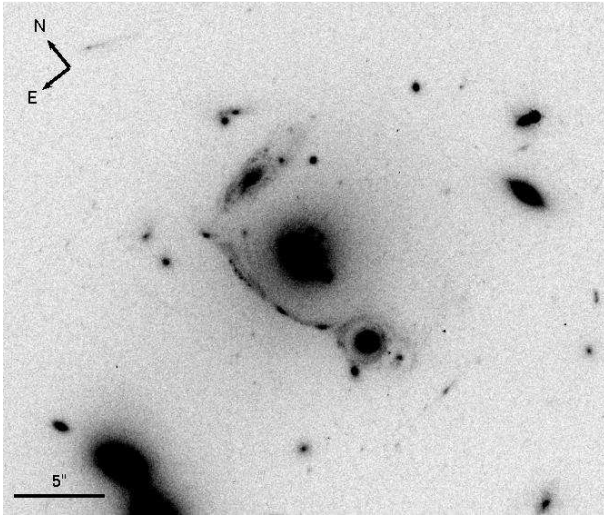


**Figure 8.**  $33'' \times 28''$  image section of a large arc found in the field of view of the high-redshift cluster RCS025242.5-150024, around a foreground galaxy.

method, the core luminosity is underestimated due to background over-subtraction, but in a consistent way for the X-ray and optical clusters. In contrast to the two previous methods, where the dominant galaxies in the cluster core are early types, in this case the color correction, applied in order to convert F606W fluxes to F814W, is less clear-cut, since fainter and undetectable dwarf galaxies may well be blue. For the range in color terms from early-type to late-type galaxies, the luminosity distributions are either consistent with being drawn from the same parent distribution (0.05 probability for the null hypothesis, “blue” color correction), to marginally consistent (0.01 probability for the null hypothesis, “red” color correction). At most (in the case of the low-redshift subsamples, and assuming the reddest color correction) the medians of these two distributions differ only by a factor of 1.6.

Overall, as shown in Table 8, the medians of the RCS and MACS cluster luminosity distributions and the results of the KS tests we applied to these distributions suggest that the RCS and

MACS cluster samples have similar optical luminosities. We note also that the MACS clusters that actually display arcs (shaded histograms in Fig. 9) are not necessarily the most luminous ones, and that there is a large overlap of their luminosities with those of RCS clusters that are much less efficient arc producers. We have also measured and compared the optical light profiles of the two samples and, within the limited range of the cluster cores covered by the ACS data, we find no significant differences.

However, stars, let alone the small fraction of the stars that dominate the optical luminosity, are a tiny component of the total cluster mass, and it is therefore plausible that the masses of the two samples are very different, despite the similar optical luminosities, with masses significantly below  $10^{15} M_{\odot}$  for the RCS clusters. A strong argument for such a mass difference is the difference in the space densities of the two samples. From the numbers of clusters and the area surveyed (see § 2), the projected density of MACS clusters is  $\sim 0.01 \text{ deg}^{-2}$ . Assuming the cluster mass function is probed correctly by X-ray surveys, only about one MACS-like massive cluster is expected in the  $\sim 100 \text{ deg}^2$  search area of the RCS survey. Based on the cluster mass function (e.g. Reiprich & Böhringer 2002), the  $\sim 1000$  clusters found in the RCS search area imply that the vast majority of these clusters have masses of  $M_{200} = 10^{14} M_{\odot}$ , an order of magnitude lower than MACS clusters.

This picture is further supported by the distributions of arc separations from the cluster centres. Since arcs occur near critical curves, the separations can roughly represent the Einstein radii of the clusters. As noted in §3 and seen in Fig. 4, the MACS clusters have arcs at  $10'' - 50''$ , with a median at  $24''$ , while the RCS arcs are generally much closer in, with a median of  $10''$ . The small Einstein radii of most of the RCS clusters with arcs are similar to those of rich groups.

A puzzling corollary of the above arguments, however, is the fact that in the small subsample of 52 RCS clusters imaged with ACS, which constitute just 5 per cent of the full RCS sample, there are as many as two clusters (RCS 141910+5326.1 and RCS 215609.1+012319) with arcs at separations implying  $20''$  Einstein radii, and hence MACS-like masses, in contrast to the expectation that of order just one such cluster exists in the *entire* RCS survey. Furthermore, despite their mass, only about half of the MACS clusters display arcs in our survey, because a galaxy in a suitable position in the source plane is required in order to produce an arc. The two large-separation RCS clusters in the HST sample would thus imply about 4 massive RCS clusters in the HST sample, and  $\sim 100$  in the full RCS sample, as opposed to the  $\sim 1$  expected from the X-ray-derived mass function. A possible explanation is that the HST RCS sample is not a fully representative selection of the RCS. Indeed, the wide arcs of the cluster RCS 141910+5326.1 above were already noted in ground-based images by Gladders et al. (2003), and it may have been included in the HST sample for this reason. Thus, the HST RCS sample could be a representative subsample of the RCS, *plus* a few of the most massive RCS clusters, and would thus be pre-biased in favor of lensing. Since, despite this bias, the X-ray-selected clusters are still much more efficient lenses, the observed arc occurrence frequency in the RCS clusters imaged with HST provides an upper limit on the RCS arc frequency as a whole.

On the other hand, Gladders et al. (2003) discussed eight potential lenses out of the full RCS sample of about 1000 clusters. With random selection, one would expect 1.1 of these eight lenses to be included among the 150 RCS clusters in the HST Snapshot sample, out of which the actually observed targets were chosen by HST schedulers. In fact, there are two of the eight Gladders et al. (2003) potential lenses among the 150 HST targets. This could be

**Table 8.** Comparison of MACS and RCS cluster luminosities

Subsample	Optical luminosity measure	KS Probability
Cluster BCG absolute magnitudes		
MACS ( $0.3 \leq z < 0.5$ )	−21.9	0.12
RCS ( $0.3 \leq z < 0.5$ )	−22	
MACS ( $0.5 \leq z < 0.7$ )	−23.8	0.35
RCS ( $0.5 \leq z < 0.7$ )	−23.6	
Cluster core luminosities (light of bright galaxies only)		
MACS ( $0.3 \leq z < 0.5$ )	1.5	0.12
RCS ( $0.3 \leq z < 0.5$ )	1.3	
MACS ( $0.5 \leq z < 0.7$ )	2.4	0.37
RCS ( $0.5 \leq z < 0.7$ )	2.2	
Cluster core luminosities (total light)		
MACS ( $0.3 \leq z < 0.5$ )	3.8	0.01
RCS ( $0.3 \leq z < 0.5$ )	2.3	
MACS ( $0.5 \leq z < 0.7$ )	4.5	0.07
RCS ( $0.5 \leq z < 0.7$ )	3.1	

Note- Optical luminosity measure indicates F606W or F814W absolute magnitudes for the BCGs, and luminosities in units of  $10^{45}$  erg s $^{-1}$  for the two measures of core optical luminosity. Probability is for the null hypothesis that a pair of distributions are not different.

the result of some slight bias in favor of known lenses, as described above, but could of course be due just to chance. We reiterate that, if the RCS sample is unbiased, our conclusion about the relatively low lensing inefficiency of RCS clusters hold. If the RCS sample was pre-biased, this conclusion is only strengthened.

The simplest explanation for our measurement of a low lensing efficiency among RCS clusters, compared to X-ray-selected clusters, is a typical RCS cluster mass that is lower by an order of magnitude. This leaves open the question of what stands behind the similarity of X-ray and RCS clusters, in terms of stellar luminosity, optical profiles, numbers of galaxies, and general optical appearance. These similarities cannot be due to chance line-of-sight projections (RCS clusters are chosen based on redshifts of the early-type galaxies that characterise dense environments, so they are, in fact, real associations), nor due to projection effects along large-scale structure “filaments” – simulations have shown that large scale structure may contribute only about 10 per cent to the cluster surface mass density (Wambsganss, Bode, & Ostriker 2005; Hilbert et al. 2007). Instead, there is a real and large variation in the total-mass-to-optical-light ratio among clusters. The low mass-to-light ratio of RCS cluster cores may be caused by a bias in favour of line-of-sight mergers in the optical selection process, a prominent and spectacular example of which is Cl0024+24 (Czoske et al. 2002). Indeed, extensive spectroscopic follow-up of RCS clusters has uncovered several cases of close projection effects of possibly physically associated systems as well as line-of-sight substructure (Gilbank et al. 2007; Cain et al. 2008).

A further effect to consider is the question of whether X-ray selection may favour the inclusion of clusters that are in the process of merging. Torri et al. (2004) have found that, during a merger, the lensing cross section is increased by a factor of 5 – 10 for a duration of a couple of hundred million years, while the X-ray luminosities of merging clusters are increased by a factors of  $\sim 5$ . A similar conclusion regarding the X-ray luminosity of clusters during mergers was reached by Randall, Sarazin, & Ricker (2002).

If X-ray-selected cluster samples indeed have a larger fraction of merging clusters, one could thus expect a larger fraction of highly efficient lenses in those samples. Thus, the masses of the X-ray-selected clusters may be systematically overestimated as well.

An interesting question is whether comparable optically and X-ray-selected cluster samples at  $z > 0.7$  also differ in their arc production efficiencies. We did not find giant arcs in any of the high-redshift RCS clusters we analyzed, even though their optical luminosities are comparable to those of the RCS clusters at low and medium redshifts. This contrasts with the results of Gladders et al. (2003) who found RCS clusters to be more efficient lenses at high redshift.

Finally, the many arcs found in the MACS low- and medium-redshift subsamples provide a statistically improved handle on the angular distribution of arcs in clusters. Our results show that arcs do form at large angular separations from cluster centres, at up to  $60''$ , in some cases. Thus, the large Einstein radius of Abell 1689 is probably not unique.

## 5 SUMMARY

We have conducted an algorithmically based search for lensed arcs in  $\sim 100$  clusters observed with HST. Our cluster sample includes an X-ray selected subsample (XBACs; MACS) and an optically selected subsample (RCS), each in a range of redshifts. Our search for giant arcs has produced 12, 17, and 13 arcs ( $l/w > 10$ ) in the XBACs, MACS low-redshift, and MACS medium-redshift subsamples, respectively. Only 2, 5, and zero arcs were found in the low-, medium-, and high-redshift RCS subsamples. The arc production efficiency of the MACS clusters is therefore higher by a factor of 5 – 10 than that of the RCS clusters. The typical Einstein radii of MACS clusters are several times larger than those of the relatively few RCS cluster that do display strong lensing. If, as we suspect, the HST sample of RCS clusters was pre-selected in a way that fa-

vored strong lenses, then these conclusions would only be strengthened.

These results constitute direct evidence, based on strong-lensing statistics, that optically selected RCS clusters are an order of magnitude less massive than X-ray selected clusters, despite their similar optical properties. This conclusion is supported by the factor-100 higher space density of RCS clusters. In the arc statistics literature to date, the observed statistics from X-ray and optical clusters have often been discussed together and interchangeably. We have demonstrated that X-ray and optically selected clusters likely probe distinct parts of the cluster mass function, and should therefore not be mixed in this way.

In a forthcoming paper, we will address arc statistics from a theoretical point of view. We will present strong lensing statistics predictions using clusters from several of the latest cosmological simulations, calculated specifically for comparison with the observed samples analyzed here. We expect that the observational database we have presented, compared to these improved new simulations, will elucidate some of the contradictions that have been encountered to date in this field.

## ACKNOWLEDGEMENTS

We thank Eran Ofek and Dovi Poznanski for their help with synthetic photometry and Keren Sahron for useful discussions. We thank the anonymous referee for constructive comments. D.M. acknowledges support by the Israel Science Foundation and by the DFG through German-Israeli Project Cooperation grant STE1869/1-1.GE625/15-1. This research has made use of NASA's Astrophysics Data System (ADS) Bibliographic Services, as well as the NASA/IPAC Extragalactic Database (NED). This work is based on observations made with the NASA/ESA Hubble Space Telescope, obtained from the data archive at the Space Telescope Science Institute. STScI is operated by the Association of Universities for Research in Astronomy, Inc. under NASA contract NAS 5-26555. HE gratefully acknowledges financial support from STScI grants GO-09722, GO-10491, and GO-10875. MB was supported by the Transregio-Sonderforschungsbereich TR 33 of the Deutsche Forschungsgemeinschaft.

## REFERENCES

- Alard C., 2006, *astro*, arXiv:astro-ph/0606757
- Allen S. W., Rapetti D. A., Schmidt R. W., Ebeling H., Morris R. G., Fabian A. C., 2008, *MNRAS*, 383, 879
- Balestra I., Tozzi P., Ettori S., Rosati P., Borgani S., Mainieri V., Norman C., Viola M., 2007, *A&A*, 462, 429
- Bartelmann M., Huss A., Colberg J. M., Jenkins A., Pearce F. R., 1998, *A&A*, 330, 1 (B98)
- Bertin E., Arnouts S., 1996, *A&AS*, 117, 393
- Bridle S. L., Eke V. R., Lahav O., Lasenby A. N., Hobson M. P., Cole S., Frenk C. S., Henry J. P., 1999, *MNRAS*, 310, 565
- Broadhurst T. J., Barkana R., 2008, *MNRAS*, 390, 1647
- Cain B., et al., 2008, *ApJ*, 679, 293
- Czoske O., Moore B., Kneib J.-P., Soucail G., 2002, *A&A*, 386, 31
- Dalal N., Holder G., Hennawi J. F., 2004, *ApJ*, 609, 50
- Dunkley J., et al., 2009, *ApJS*, 180, 306
- Ebeling H., Voges W., Böhringer H., Edge A. C., Huchra J. P., Briel U. G., 1996, *MNRAS*, 281, 799
- Ebeling H., Edge A. C., Henry J. P., 2001, *ApJ*, 553, 668
- Ebeling H., Barrett E., Donovan D., 2004, *ApJ*, 609, L49
- Ebeling H., Barrett E., Donovan D., Ma C.-J., Edge A. C., van Speybroeck L., 2007, *ApJ*, 661, L33
- Ebeling H., Ma C. J., Kneib J.-P., Jullo E., Courtney N. J. D., Barrett E., Edge A. C., Le Borgne J.-F., 2009, *MNRAS*, 395, 1213
- Edge A. C., Ebeling H., Bremer M., Röttgering H., van Haarlem M. P., Rengelink R., Courtney N. J. D., 2003, *MNRAS*, 339, 913
- Fedeli C., Bartelmann M., Meneghetti M., Moscardini L., 2008, *A&A*, 486, 35
- Flores R. A., Maller A. H., Primack J. R., 2000, *ApJ*, 535, 555
- Gilbank D. G., Yee H. K. C., Ellingson E., Gladders M. D., Barrientos L. F., Blindert K., 2007, *AJ*, 134, 282
- Gilbank D. G., Yee H. K. C., Ellingson E., Gladders M. D., Loh Y.-S., Barrientos L. F., Barkhouse W. A., 2008, *ApJ*, 673, 742
- Gladders M. D., Hoekstra H., Yee H. K. C., Hall P. B., Barrientos L. F., 2003, *ApJ*, 593, 48
- Gladders M. D., Yee H. K. C., 2005, *ApJS*, 157, 1
- Hansen S. M., McKay T. A., Wechsler R. H., Annis J., Sheldon E. S., Kimball A., 2005, *ApJ*, 633, 122
- Hennawi J. F., Dalal N., Bode P., Ostriker J. P., 2007, *ApJ*, 654, 714
- Hennawi J. F., et al., 2008, *AJ*, 135, 664
- Hilbert S., White S. D. M., Hartlap J., Schneider P., 2007, *MNRAS*, 382, 121
- Horesh A., Ofek E. O., Maoz D., Bartelmann M., Meneghetti M., Rix H.-W., 2005, *ApJ*, 633, 768 (H05)
- Jing Y. P., Suto Y., 2002, *ApJ*, 574, 538
- Kartaltepe J. S., Ebeling H., Ma C. J., Donovan D., 2008, *MNRAS*, 389, 1240
- Kauffmann G., Colberg J. M., Diaferio A., White S. D. M., 1999, *MNRAS*, 303, 188
- Kinney A. L., Calzetti D., Bohlin R. C., McQuade K., Storchi-Bergmann T., Schmitt H. R., 1996, *ApJ*, 467, 38
- Koester B. P., et al., 2009, arXiv, arXiv:0903.2478
- Limousin M., et al., 2007, *ApJ*, 668, 643
- Lenzen F., Schindler S., Scherzer O., 2004, *A&A*, 416, 391
- Ma C.-J., Ebeling H., Donovan D., Barrett E., 2008, *ApJ*, 684, 160
- Ma C.-J., Ebeling H., Barrett E., 2009, *ApJ*, 693, L56
- Mantz A., Allen S. W., Ebeling H., Rapetti D., 2008, *MNRAS*, 387, 1179
- Mantz A., Allen S. W., Rapetti D., Ebeling H., 2009, arXiv, arXiv:0909.3098
- Mantz A., Allen S. W., Ebeling H., Rapetti D., Drlica-Wagner A., 2009, arXiv, arXiv:0909.3099
- Meneghetti M., Bolzonella M., Bartelmann M., Moscardini L., Tormen G., 2000, *MNRAS*, 314, 338
- Meneghetti M., Bartelmann M., Moscardini L., 2003, *MNRAS*, 346, 67
- Navarro J. F., Frenk C. S., White S. D. M., 1996, *ApJ*, 462, 563
- Neto A. F., et al., 2007, *MNRAS*, 381, 1450
- Oguri M., Lee J., Suto Y., 2003, *ApJ*, 599, 7
- Oguri M., Blandford R. D., 2009, *MNRAS*, 392, 930
- Puchwein E., Bartelmann M., Dolag K., Meneghetti M., 2005, *A&A*, 442, 405
- Randall S. W., Sarazin C. L., Ricker P. M., 2002, *ApJ*, 577, 579
- Reiprich T. H., Böhringer H., 2002, *ApJ*, 567, 716
- Richard J., et al., 2007, *ApJ*, 662, 781
- Rozo E., Nagai D., Keeton C., Kravtsov A., 2008, *ApJ*, 687, 22
- Sadeh S., Rephaeli Y., 2008, *MNRAS*, 388, 1759
- Sand D. J., Treu T., Ellis R. S., Smith G. P., 2005, *ApJ*, 627, 32

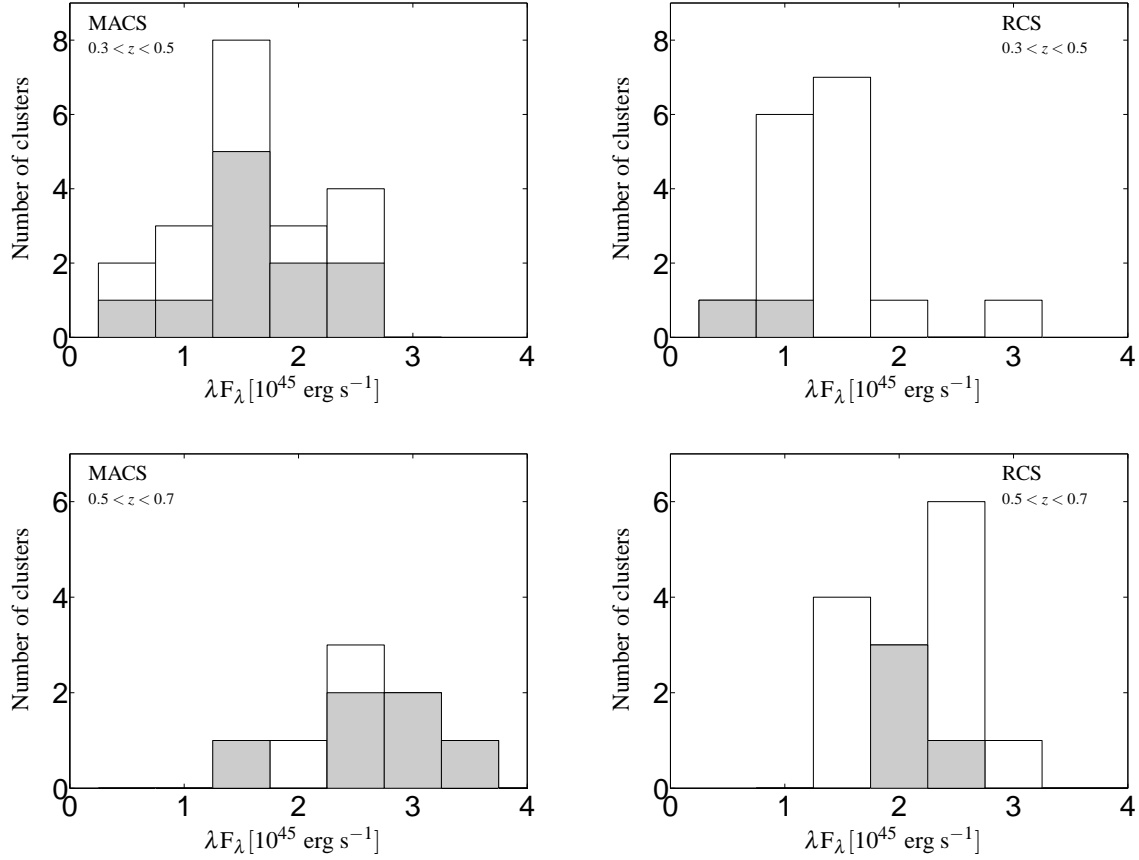


**Figure 9.** Distributions of the MACS (left) and RCS (right) core optical luminosities at low redshift (top) and medium redshift (bottom) measured using galaxies brighter than  $m_{F814W} = 24$ . Shaded histograms designate the clusters that display one or more lensed arcs.

- Seidel G., Bartelmann M., 2007, A&A, 472, 341  
Smail I., et al., 2007, ApJ, 654, L33  
Smith G. P., Kneib J.-P., Smail I., Mazzotta P., Ebeling H., Czoske O., 2005, MNRAS, 359, 417  
Stott J. P., Smail I., Edge A. C., Ebeling H., Smith G. P., Kneib J.-P., Pimbblet K. A., 2007, ApJ, 661, 95  
Torri E., Meneghetti M., Bartelmann M., Moscardini L., Rasia E., Tormen G., 2004, MNRAS, 349, 476  
Vikhlinin A., et al., 2009, ApJ, 692, 1060  
Voges W., et al., 1999, A&A, 349, 389  
Voit G. M., 2005, RvMP, 77, 207  
Wambsganss J., Bode P., Ostriker J. P., 2004, ApJ, 606, L93  
Wambsganss J., Bode P., Ostriker J. P., 2005, ApJ, 635, L1  
Zaritsky D., Gonzalez A. H., 2003, ApJ, 584, 691  
Zitrin, A., Broadhurst, T., Barkana, R., Rephaeli, Y., & Benitez, N. 2010, arXiv:1002.0521  
Zitrin A., Broadhurst T., Rephaeli Y., Sadeh S., 2009, arXiv, arXiv:0907.4232

